Journal of Luminescence 235 (2021) 118050

Contents lists available at ScienceDirect

Journal of Luminescence

journal homepage: http://www.elsevier.com/locate/jlumin

Synthesis, structure and photoluminescent properties of Eu:Gd_2O_3 nanophosphor synthesized by cw CO_2 laser vaporization

Anton I. Kostyukov [a,*], Valeriy N. Snytnikov [b], Vladimir N. Snytnikov [b], Marianna I. Rakhmanova [c], Nadezhda Y. Kostyukova [a,d,e], Arcady V. Ishchenko [a,b], Svetlana V. Cherepanova [a,b], Alexander S. Krylov [f], Aleksandr S. Aleksandrovsky [f,g]

[a] Novosibirsk State University, Pirogova Str. 2, 630090, Novosibirsk, Russia
[b] Boreskov Institute of Catalysis SB RAS, Lavrentieva Ave. 5, 630090, Novosibirsk, Russia
[c] Nikolaev Institute of Inorganic Chemistry SB RAS, Akad. Lavrentiev Ave. 3, 630090, Novosibirsk, Russia
[d] Institute of Laser Physics SB RAS, Lavrentyev Ave. 15b, 630090, Novosibirsk, Russia
[e] Novosibirsk State Technical University, K. Marx Ave. 20, 630073, Novosibirsk, Russia
[f] Kirensky Institute of Physics Federal Research Center KSC SB RAS, Krasnoyarsk, 660036, Russia
[g] Department of Photonics and Laser Technology, Siberian Federal University, Krasnoyarsk, 660041, Russia

ARTICLE INFO

Keywords:
Photoluminescence
Eu^{3+} ions
Monoclinic Gd_2O_3
Nanophosphors
Laser vaporization

ABSTRACT

Europium doped Gd_2O_3 sphere-like nanoparticles with $d_m = 9.3 \pm 3.5$ nm were synthesized by cw CO_2 laser vaporization technique in a flowing mixture of argon and oxygen. According to XRD data, the Eu:Gd_2O_3 nanoparticles crystallize in the monoclinic symmetry class (*C2/m* space group). High-resolution luminescence spectroscopy study showed that the ultra-narrow $^5D_0 \rightarrow {}^7F_0$ transition of Eu^{3+} demonstrates only two peaks corresponding to two inequivalent C_s positions of Eu^{3+} ion in monoclinic Gd_2O_3 lattice that is explained by the peculiarities of local environment of Eu^{3+} ion at these sites. The hypersensitive transition $^5D_0 \rightarrow {}^7F_2$ dominates in the spectrum and is expanded to the red part of the spectrum in comparison with cubic Eu:Gd_2O_3 due to intense transitions terminating at higher-lying components of the crystal-field-split $^7F_2$ state. In the luminescence spectrum, an additional weak band with the maximum at 407 nm corresponding to the electronic transitions $4f^65\ d^1(^7F_J) \rightarrow 4f^7(^8S_{7/2})$ of Eu^{2+} was detected. The obtained values of chromaticity coordinates and absolute quantum yield are (0.644; 0.325) and ca. 1%, respectively. The phase transformations have been investigated using differential scanning calorimetry and thermogravimetry (50–1400 °C). After annealing in air at 700 °C, the monoclinic symmetry class of the Eu:Gd_2O_3 nanoparticles is preserved and the particle size increases to $d_m = 17.8 \pm 6.1$ nm. After annealing, the chromaticity coordinates (0.659; 0.334) and absolute quantum yield (ca. 4%) can be obtained using red phosphor based on monoclinic Gd_2O_3:Eu^{3+}. The lifetime of the excited $^5D_0$ state of Eu^{3+} in the annealed nanoparticles is longer than that in the as-synthesized nanoparticles, due to the suppression of nonradiative decay after annealing.

1. Introduction

Nowadays investigations of the new red phosphors are of interest to the material research community. The rare earth sesquioxides are one of the typical phosphor matrices for activators emitting in the red spectral region. Among such activators, trivalent europium is most frequently used. The red color of phosphors with Eu^{3+} activator is determined by the distribution of intensities between luminescence bands originating from the higher-lying $^5D_0$ state and terminating at the low-lying ^7F_J (J = 0–6) states. The hypersensitive $^5D_0 \rightarrow {}^7F_2$ transition typically dominates in efficient phosphors since its large oscillator strength induced by the crystal field is favorable to prevent radiationless losses. The intensity distribution of transitions between individual crystal-field-split subcomponents within this band varies from host to host, and typically the maximum of emission lies between 610 and 620 nm [1,2].

Among the rare earth sesquioxides, the Gd_2O_3 host for Eu^{3+} is attractive due to its optical properties, good chemical durability, thermal stability, and low phonon energy. Moreover, gadolinium is a rare

* Corresponding author.
E-mail address: ant.kostyukov@mail.ru (A.I. Kostyukov).

https://doi.org/10.1016/j.jlumin.2021.118050
Received 9 December 2020; Received in revised form 16 February 2021; Accepted 9 March 2021
Available online 11 March 2021

earth element that has paramagnetic properties and can be used in magnetic resonance imaging (MRI), fluorescence imaging, X-ray computed tomography (CT), and neutron capture therapy for cancers [3–8]. This makes it possible to develop compounds based on Gd_2O_3 as potentially bifunctional materials with both the luminescent and magnetic properties.

Three structures were found in the sesquioxides, including Gd_2O_3, known as hexagonal ($P3m1$), cubic ($Ia3$), and monoclinic ($C2/m$) phases. The most comprehensive studies of luminescence were made for Eu^{3+} in cubic c-Gd_2O_3 [4,5,7–16]. In c-Gd_2O_3:Eu^{3+}, the structure of luminescence bands originating from the $^5D_0$ state and terminating at the ^7F_J (J = 0–6) states, in particular, the most intense emission bands of the $^5D_0 \rightarrow {}^7F_2$ with λ_{max} of ca. 611 nm, is due to centrosymmetric C_{3i} and non-centrosymmetric C_2 anionic environments of the Eu^{3+}. The luminescence of monoclinic m-Gd_2O_3:Eu^{3+} obtained by combustion synthesis, high-pressure high-temperature synthesis, and high-temperature flame spray pyrolysis was investigated in Refs. [17–24]. The modification of Eu^{3+} luminescence spectra in the monoclinic polymorph with respect to the cubic one was shown. Three nonequivalent sites of C_s local symmetry (A, B, and C) in m-Gd_2O_3:Eu^{3+} were identified with high-resolution luminescence spectroscopy.

In recent decades, attention has been paid to the study of nanoparticles due to a qualitative change in the physical and chemical properties of materials at the nanoscale, especially in the size range of 10 nm. The variety of morphologies and sizes is widely researched due to their potential applications in various industries [25,26]. Nanophosphors, including Gd_2O_3, have been produced by many synthesis techniques, including solution combustion, single-source precursor, coprecipitation, flame spray pyrolysis, sol-gel, etc. Previously, terbium doped m-Gd_2O_3 nanoparticles were prepared by laser ablation in liquid using a microsecond Nd:YAG laser [6]. In this study, the CO_2 laser vaporization (LAVA) technique was used for the preparation of Eu:Gd_2O_3 nanophosphor. The advantage of the LAVA method is the possibility to control multiple parameters of a setup during the synthesis of softly agglomerated nanoparticles with multicomponent composition [27–31]. This opens the possibility of intentional control over such properties of the produced materials as the particle size distribution, composition, and stoichiometry. Besides, chemical impurities are virtually absent in the final nanomaterials, in contrast to the chemical synthesis. We have previously shown that the europium doped Y_2O_3 spherical nanoparticles with the diameter of ca. 10 nm obtained via cw CO_2 LAVA are crystallizing in the monoclinic symmetry class ($C2/m$ space group) [31]. The europium doped Gd_2O_3 nanoparticles obtained by the LAVA method are expected to crystallize in the same class of symmetry. The structure, morphology, and luminescent properties of such nanoparticles have not been previously analyzed in detail.

The aim of the present study is to obtain nanoparticles of europium doped Gd_2O_3 via cw CO_2 laser vaporization in a flowing mixture of argon and oxygen and to investigate the morphology as well as the structural and luminescent properties of the obtained nanophosphor by means of high-resolution spectroscopy.

2. Experimental techniques

2.1. Synthesis of europium doped Gd_2O_3 nanoparticles

Eu:Gd_2O_3 ceramic targets for vaporization were prepared using nitrate salts $Eu(NO_3)_3{\cdot}6H_2O$ (99.7%) and $Gd(NO_3)_3{\cdot}6H_2O$ (99.7%), respectively. Purity of the starting materials was determined by XRF analysis. The synthesis of nanoparticles included a preliminary mechanical mixing of the initial salts followed by their drying, calcination and press molding to obtain pelletized targets from the powders; after that, nanopowders were produced by laser vaporization of the targets.

Before obtaining the mechanical mixtures, loss on ignition (LOI) was estimated at 550 °C for each of the initial salts. To this end, 1 g samples of each salt were dried under similar conditions in an air flow at 110 °C/6 h and then calcined stepwise at 250 °C/2 h and 550°C/4 h. The acquired LOI data were used to calculate the amount of initial components (wt.%) required for the synthesis of samples with the desired composition $Gd_{1.9}Eu_{0.1}O_3$ (10 wt% Eu). After estimating the LOI values, necessary amounts of the initial salts were mixed for 30 min to ensure the best distribution of the Eu-containing component. The prepared mixtures were then dried in an air flow at 110°C/6 h and calcined stepwise at 250°C/2 h and 550°C/4 h. After that, samples with the composition $Gd_{1.9}Eu_{0.1}O_3$ were loaded in a vacuum press mold to obtain pellets with the diameter 18 mm and thickness 2.6 mm. Relative density of the pellets (related to zero porosity) was 45–55%. Prior to vaporization, the pellets were additionally annealed at 850 °C during 4 h. The phase composition of the target was controlled by XRD. According to XRD data, the initial $Gd_{1.9}Eu_{0.1}O_3$ ceramic target was represented by the well-known cubic *Ia-3* phase.

Europium doped Gd_2O_3 nanoparticles were synthesized in a two-chamber laser vaporization setup [29–31]. The setup consists of a 16 L external sealed steel chamber operating in a pressure range of 0.1 Pa–200 kPa, vacuum post, laser radiation input, and systems for optical control, target control, gas feeding, and chamber pressure control. Eu:Gd_2O_3 ceramic targets were vaporized from a copper crucible in the internal chamber with a coaxial labyrinth scheme for particle separation in a gas flow. Particles entrained by the flow were deposited on ash-free paper filters with the diameter of 110 mm, which separate the vaporization chamber from the vacuum pumping channel. The vaporization process is visually controlled through a cylindrical quartz housing of the internal chamber using a glass lens, which serves also as a window of the external chamber. Vaporization took place when continuous radiation of a CO_2 laser with a 103 W power was focused on the target (radiation wavelength 10.6 μm, generation power up to 110 W on one TEM_{00} transverse mode, output beam diameter 8 mm, divergence in the far-field region 3×10^{-3} rad) at a spot with the diameter 0.4–0.5 mm, where the boiling zone formed; the melting zone had the diameter of 2–3 mm. Vaporized oxides and radicals were cooled and condensed in a flow of Ar (99.998%) and O_2 (99.7%) gases, which were fed through the nozzle coaxially with the laser beam. The typical gas flow rate was 130 and 15 L/h for Ar and O_2, respectively. Vaporization was performed at a 10 kPa (0.1 bar) pressure of the Ar and O_2 gas mixture in the chamber. The chamber with the target was preliminarily sealed and evacuated using a backing pump to obtain a residual pressure of 0.02 Pa. Finally, after cooling the chamber to room temperature and its opening, a sample of Eu:Gd_2O_3 nanopowders was collected from the filter, ground to obtain the fine mesh powders, and studied by physicochemical methods. At the specified conditions of Eu:Gd_2O_3 nanoparticles synthesis by laser vaporization, the rate of nanopowder vaporization and deposition on the filer was 860 mg/h. In addition, a part of the produced $Gd_{1.9}Eu_{0.1}O_3$ nanopowder was annealed in air at 700°C for 4 h. Schematic diagram of the synthesis process of Eu:Gd_2O_3 nanoparticles is shown on Fig. 1.

2.2. Characterization of europium doped Gd_2O_3 nanoparticles

Elemental analysis of the sample was made using X-ray fluorescence spectroscopy (XRF) on an ARL – Advant'x analyzer (Thermo Scientific) with the Rh anode of the X-ray tube. Local analysis of elemental composition of the sample was performed on an energy-dispersive EDS spectrometer QUANTAX 200-TEM (Bruker) with a XFLASH detector at energy resolution of ca. 130 eV (in *Supplementary material (SM)*). The morphology of Eu:Gd_2O_3 nanoparticles was characterized by high-resolution transmission electron microscopy (HRTEM) on a JEM-2010 (JEOL) electron microscope and a Themis-Z3.1 instrument (TFS) equipped with a X-FEG monochromator and CS/S double corrector at accelerating voltage 200 kV. Samples were deposited by an ultrasonic disperser onto standard carbon-coated copper grids, which were fixed in a holder and introduced in the chamber of electron microscope. Phase composition of the Eu:Gd_2O_3 nanoparticles was revealed by X-ray

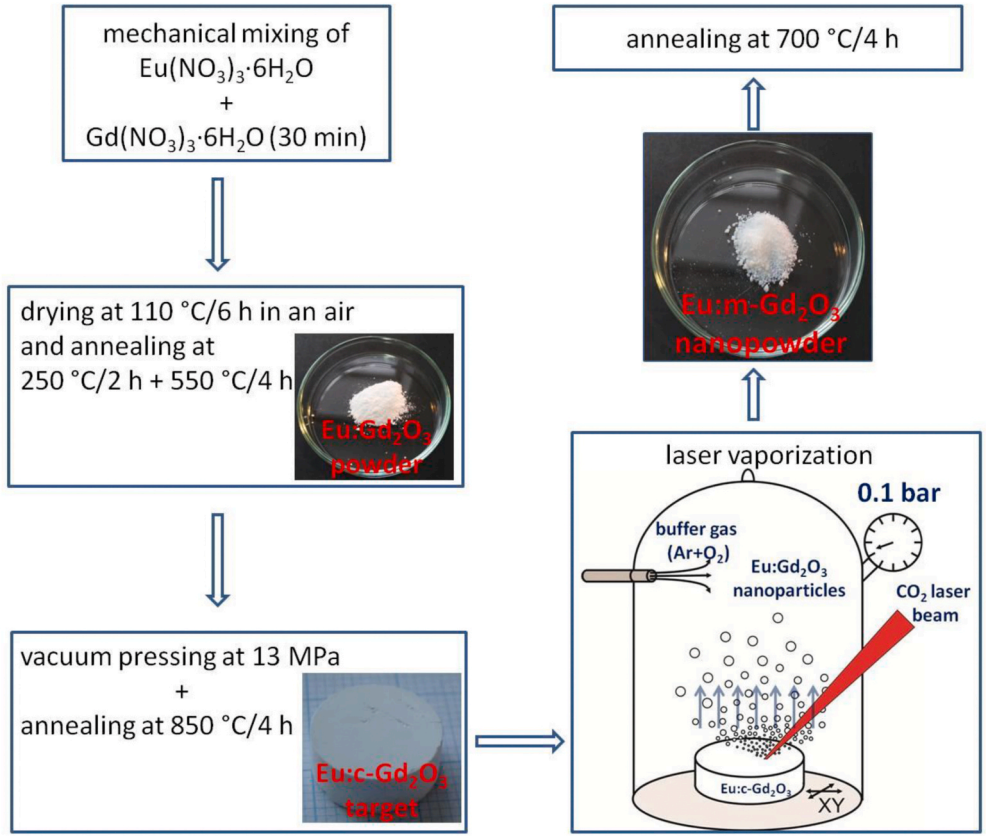

Fig. 1. Schematic diagram of the synthesis process of Eu:Gd_2O_3 nanoparticles.

diffraction (XRD) analysis. X-ray diffraction patterns were recorded on a Bruker D8 diffractometer using a CuK_α source and scanning over the range of reflection angles $2\theta = 10–75^\circ$ with a 0.05° step and accumulation time 3 s. Lattice constants and average crystallite sizes were determined by Rietveld refinement with use of TOPAS software (Bruker, Germany). Specific surface area (S_{sp}) of Eu:Gd_2O_3 nanoparticles was calculated according to BET using low-temperature nitrogen adsorption at 77 K on a DigiSorb- 2600 (Micromeritics) automated volumetric instrument. All the samples were subjected to thermal pretreatment in vacuum at 200 °C and residual pressure 10^{-4} mm Hg for 5 h. Thermal analysis of the sample was carried out using an STA 449C Jupiter (NETZSCH) instrument for synchronous thermal analysis, which combines differential thermal analysis (DTA) and thermogravimetry (TG) in a single measurement. Samples were examined in a corundum crucible using an oxidizing atmosphere. Air was fed to the chamber with the sample at a rate of 30 ml/min. An inert gas (He) was delivered to the weighting unit at a rate of 20 ml/min. The sample was heated at a rate of 2°C/min from room temperature to 50°C and held at this temperature for 60 min. This was followed by the temperature-programmed heating to 1400°C at a rate of 10°C/min.

Steady-state emission and excitation spectra and photoluminescence lifetimes were measured using a Horiba Jobin Yvon Fluorolog 3 spectrometer equipped with a 450 W Xe lamp, Czerny–Turner double grating (1200 grooves per mm) excitation and emission monochromators, and an FL-1073 PMT detector. Emission spectra were recorded from 360 to 800 nm and corrected for the spherical response of the monochromators and the detector sensitivity using typical correction spectra provided by the manufacturer. For an absolute quantum yield of solid sample (PLQYs) measurements, a Spectralon covered G8 integration sphere (GMP SA, Switzerland) was coupled to the spectrometer. According to our estimates, a consistent experimental error for the PLQYs measurements did not exceed 15%. High-resolution luminescence spectra were obtained using a Horiba JobinYvon T64000 spectrometer and GaN laser excitation source at the central wavelength of 408 nm.

3. Results and discussion

3.1. Morphological, structural and thermal analysis

As shown by the elemental analysis performed by XRF, after vaporization of the $Gd_{1.9}Eu_{0.1}O_3$ ceramic target, Eu enters the composition of the produced Gd_2O_3 nanoparticles with the concentration of 10.46 ± 0.13 wt%. The Eu concentration chosen for the study is close to the range of values (≤7 mol.%) used in Refs. [14,15] for Eu:Gd_2O_3 with the cubic structure. At such a concentration, the concentration quenching is absent, and hence the highest photoluminescence emission intensity of Eu^{3+} is reached.

Multiphase or oxide nanoparticles with the mixed composition are currently synthesized using the co-LAVA method [27–31]. This implies simultaneous vaporization of a mixture of at least two initial homogeneous powders. The composition of the resulting nanoparticles depends on the individual characteristics of each initial component, its thermophysical properties, reactivity, and the ratio of components upon mixing. According to the literature, the interaction of IR radiation with a substance having a power density below 1 MW/cm^2 is predominantly the thermal interaction. At atmospheric pressure, the typical melting and boiling points for Eu_2O_3 and Gd_2O_3 are $T_m = 2290$ °C, $T_b = 3790$ °C, and $T_m = 2350$ °C, $T_b = 3280$ °C, respectively. The difference in T_m and T_b for the initial compounds is the main cause for depletion of the component with a higher vaporization rate. Detailed XRF and EDX studies of the produced nanomaterial revealed that the content of Eu and Gd in the Eu:Gd_2O_3 nanopowder depends on the number of vaporization cycles of the initial ceramic pellet.

After vaporization of the initial target, substantial changes occur in the structure and morphology of Eu:Gd_2O_3. Fig. 2a and b displays HRTEM images of the obtained as-synthesized Eu:Gd_2O_3 nanoparticles

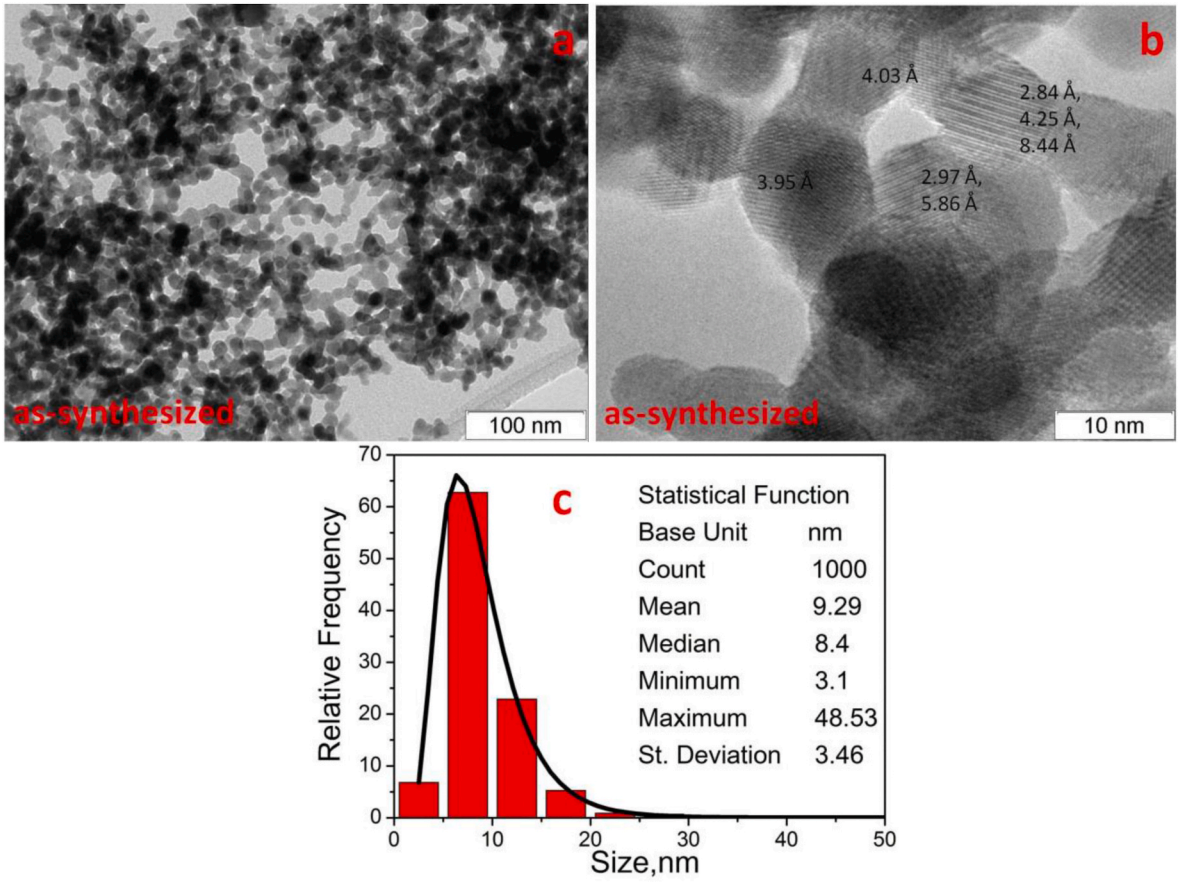

Fig. 2. a, b - HRTEM images of as-synthesized Eu:Gd_2O_3 nanoparticles with interplanar spacing (**b**); **c** – the frequency based particle diameter distribution of the nanoparticles (log normal (black curve) distribution).

and the frequency based particle diameter distribution, **Fig. 2c.**

TEM images of the Eu:Gd_2O_3 sample demonstrate that the particles have a sphere-like form and are represented by spherically 3D nanocrystallites. The mean particle diameters d_m and standard deviation σ were calculated from size histograms. For the Eu:Gd_2O_3 sample, the mean size value and its standard deviation are equal to $d_m = 9.3 \pm 3.5$ nm. The as-prepared nanopowder has a high crystallinity. HRTEM images (Fig. 2c) of the sample show interplanar distances that can be attributed mainly to monoclinic Eu:Gd_2O_3 (PDF# 42–1465). **Fig. S1a, b** show also the local analysis data on the elemental composition of Eu:Gd_2O_3 sample. According to EDX data, Eu:Gd_2O_3 nanoparticles have a composition with the Gd/Eu atomic ratio of ca. 89.72/10.28 (averaged over different local parts of the sample). Individual Eu_2O_3 particles were not detected by EDX.

After annealing of the Eu:Gd_2O_3 sample at 700°C, morphological changes occur due to agglomeration of nanoparticles, Fig. 3a and b. The particle diameter distribution (Fig. 3c) shows that the agglomeration is more pronounced for smaller nanoparticles. The average particle size increases to $d_m = 17.8 \pm 6.1$ nm. Fig. 3 shows that the crystalline quality of monoclinic phase also increases because the atom moves to the favorable position. The interplanar distances in the sample can also be attributed mainly to monoclinic Eu:Gd_2O_3 (PDF# 42–1465).

Rietveld refinement showed that all peaks on the XRD patterns of as-synthesized Eu:Gd_2O_3 and the sample annealed at 700 °C can be fitted by monoclinic cell (*C2/m* space group) with lattice constants close to those of Gd_2O_3 (PDF#42–1465), Fig. 4 and Table 1. However, one can see that lattice constants and, consequently, unit cell volumes of Eu:Gd_2O_3 are a little bit larger than these parameters of pure Gd_2O_3 because the ionic radius of Eu^{3+} (1.07 Å) is higher than that of Gd^{3+} one (1.05 Å).

In addition, average particle sizes *D* and microstrain (a local deviation of d-spacings from the average value) charactered by the parameter ε were determined with the use of Rietveld refinement. In as-synthesized sample, the average particle size is ~9 nm. The ε value is very high ($\varepsilon = 0.015$) for as-synthesized sample. The origin of high values of microstrain are usually point defects like interstitial or missing atoms, or substitution with different atoms. One-dimensional defects, like screw dislocations, or two-dimensional defects like twin boundaries may also cause microstrain, e.g. if the atoms at the boundary need to be slightly displaced in order to match the lattices of both domains. Annealing at 700 °C leads to the increase in particle sizes from 9 nm to 19 nm) and reduction of microstrain from 0.015 to 0.007. Main parameters of processing and refinement of the Eu:Gd_2O_3 nanoparticles are presented in Table 1. Rietveld refinement of coordinates of cationic positions is presented in Table S1 *(SM)*.

Thus, the cubic crystalline structure of the initial ceramic target Eu:c-Gd_2O_3 is destroyed upon vaporization, and under the conditions of nanoparticles' formation within the chamber the monoclinic structure is formed with probability close to 100% due to an additional hydrostatic pressure component, resulting from the Gibbs-Thomson effect [32] under the indicated conditions. Similar results on the synthesis of monoclinic Eu_2O_3 and Y_2O_3 nanoparticles are reported in Refs. [32,33]. The similar case is the formation of crystalline films via PLD, when initial state of the target (either ceramics or glassy one) plays no role in the nature of the forming film [34].

Fig. 5 displays thermal analysis data for as-synthesized m-Eu:Gd_2O_3 nanoparticles measured in the temperature range 50–1400 °C in air. As seen in Fig. 5, an endothermic effect with a maximum at 108 °C is observed in the temperature region of 50–200 °C, which may be caused by the removal of adsorbed water from the surface of nanoparticles [8, 35–37]. Weight losses in this region are equal to 2.6 wt%. In the region

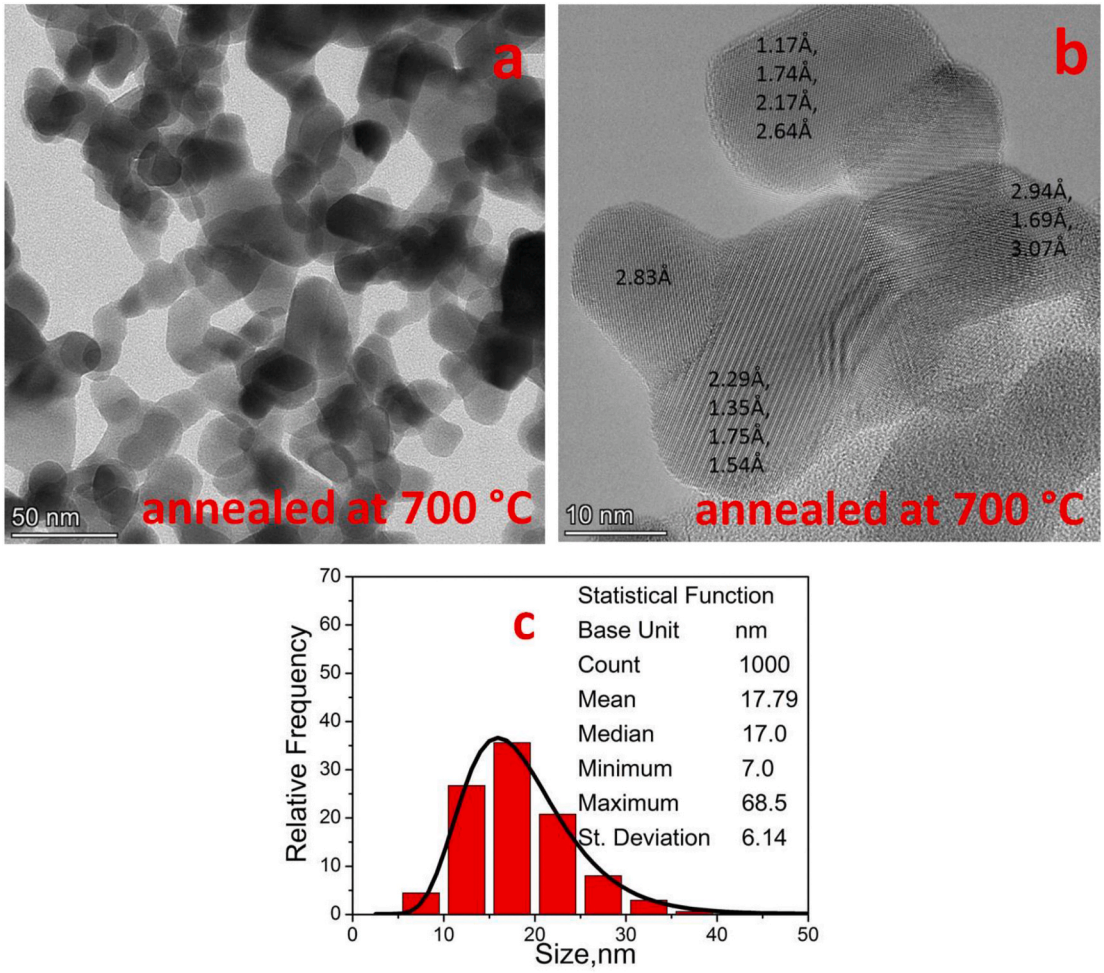

Fig. 3. a, b - HRTEM images of Eu:Gd_2O_3 nanoparticles annealed at 700 °C with interplanar spacing (**b**); **c** – the frequency based particle diameter distribution of the nanoparticles (log normal (black curve) distribution).

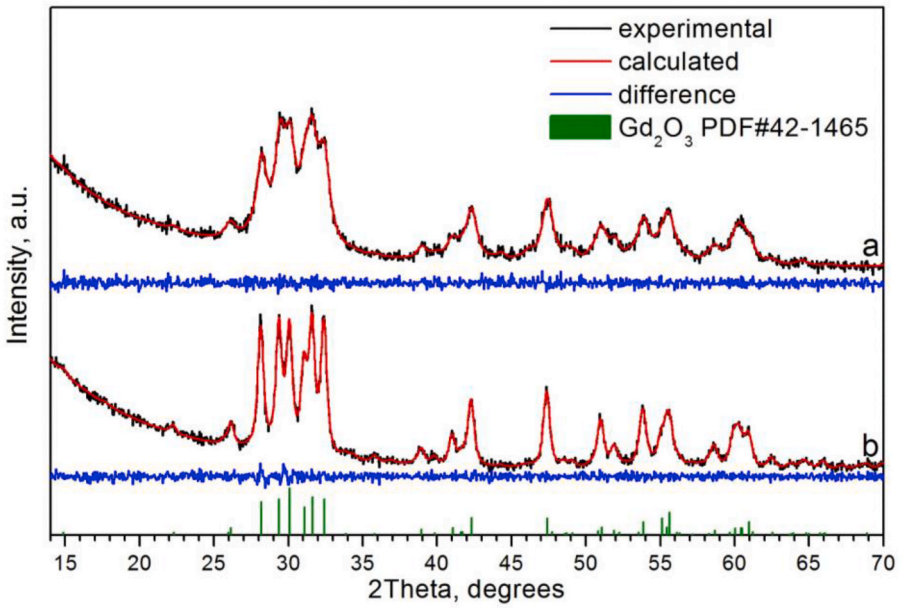

Fig. 4. Rietveld refinement of the XRD patterns of Eu:Gd_2O_3 nanoparticles:. (a) as-synthesized, R = 2.2%; (b) annealed at 700 °C, R = 2.4%. Blue line is the difference between experimental and simulated patterns.

Table 1
Lattice constants of monoclinic unit cell *a*, *b*, *c*, *β*, volumes *V*, average sizes *D* of Eu:Gd_2O_3 nanoparticles and microstrain *ε* (according to XRD).

Compound	a, Å	b, Å	c, Å	β, °	V, Å^3	D, nm	ε
as-synthesized	14.094(1)	3.581(1)	8.778(1)	100.2(1)	436.1(3)	9	0.015
annealed at 700 °C	14.103(2)	3.583(1)	8.778(1)	100.1(1)	436.6(2)	19	0.007
PDF#42-1465	14.09	3.576	8.769	100.08	435.24	–	–

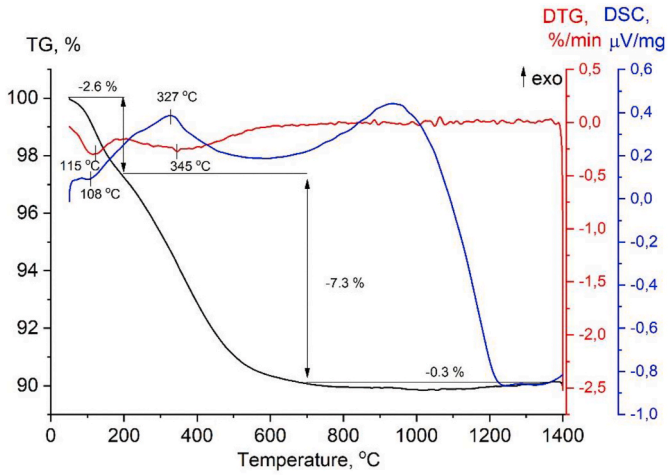

Fig. 5. TG, DTG and DTA curves of as-synthesized Eu:Gd_2O_3 nanoparticles.

of 200–700 °C, there is an extended exothermic peak with a distinct maximum at 327 °C and a shoulder near 200 °C, which are caused by the removal of adsorbed CO and CO_2 molecules, respectively [8,36,37]. Weight losses in this region are equal to 7.3 wt%. One can see in Fig. 5 that the main part of organic molecules is removed from the sample upon heating up to ca. 800 °C. According to Ref. [38], the removal of a small NO amount is observed also for monoclinic Eu:Y_2O nanoparticles at 200–350 °C and 550–700 °C. A broad exothermic effect in the region of 700–1200 °C with the maximum near 900 °C may be caused by the transformation from monoclinic to cubic phase. Accordingly, 700 °C was chosen as the annealing temperature. Total weight losses for the sample at 1400 °C are equal to 10.2 wt%. Since nanoparticles are synthesized in the vaporization-condensation chamber at a constant pumping of Ar as a buffer gas, the adsorption of water and organic molecules on the surface of Eu:Gd_2O_3 nanoparticles occurs after the removal of the sample from the chamber and proceeds via the entrainment of water vapor and organic molecules from the ambient atmosphere by the highly developed surface of nanoparticles.

3.2. Luminescent analysis

3.2.1. Emission study

Fig. 6 displays PL spectra of as-synthesized m-Eu:Gd_2O_3 and m-Eu:Gd_2O_3 samples annealed at 700 °C in comparison with that of the initial cubic Eu:Gd_2O_3 sample. The PL spectra were obtained at $\lambda_{ex} = 270$ nm. The luminescence spectrum of the as-synthesized Eu:Gd_2O_3 nanoparticles excited at $\lambda_{ex} = 270$ nm is dominated by the intraconfigurational 4f – 4f transitions of Eu^{3+} ions covering the 570–750 nm range.

The bands observed in the ranges 570–588, 588–605, 605–644, 644–674 and 674–725 nm correspond to transitions from the excited $^5D_0$ level of Eu^{3+} ion to sublevels of the ground state ^7F_J (J = 0–4). The 570–588 nm range contains the $^5D_0 \rightarrow {}^7F_0$ transition, which is strictly forbidden in the presence of local mirror symmetry according to the standard Judd-Ofelt theory. For a single inequivalent site of Eu^{3+} ion within a crystal structure, this transition contains a single line with the intensity that typically is the lowest among all bands starting from the $^5D_0$ level. The local symmetry as low as C_{nv}, C_n or C_s makes this transition visible [1,2]. According to earlier studies, in the monoclinic Gd_2O_3 nanoparticles, there are three nonequivalent point sites of Eu^{3+} usually referred to as A, B, and C, each of them of C_s symmetry [17–24]. In such sites, Eu^{3+} is seven-fold coordinated. The coordination of two possible Eu^{3+} ion sites can be described by six oxygens at the apexes of a trigonal prism with the seventh oxygen atom along a normal to the face [20]. The spectral region of the ultra-narrow transition $^5D_0 \rightarrow {}^7F_0$ of trivalent Eu^{3+} ions is presented in Fig. 7 in more detail. The luminescence spectrum of the monoclinic Eu:Y_2O_3 nanoparticles prepared in Ar is given in Fig. 7 for comparison.

For m-Eu:Gd_2O_3, two pronounced ultra-narrow transitions are detected that are peaking at 578.5 and 581.9 nm. The neighboring peak at 584.2 nm (observable in Fig. 6) must be ascribed to the manifold of $^5D_1 \rightarrow {}^7F_3$ transitions. Therefore, luminescence from only two inequivalent sites of Eu in m-Eu:Gd_2O_3 can be seen in the luminescence at $^5D_0 \rightarrow {}^7F_0$ transitions. The explanation for this fact is as follows. As

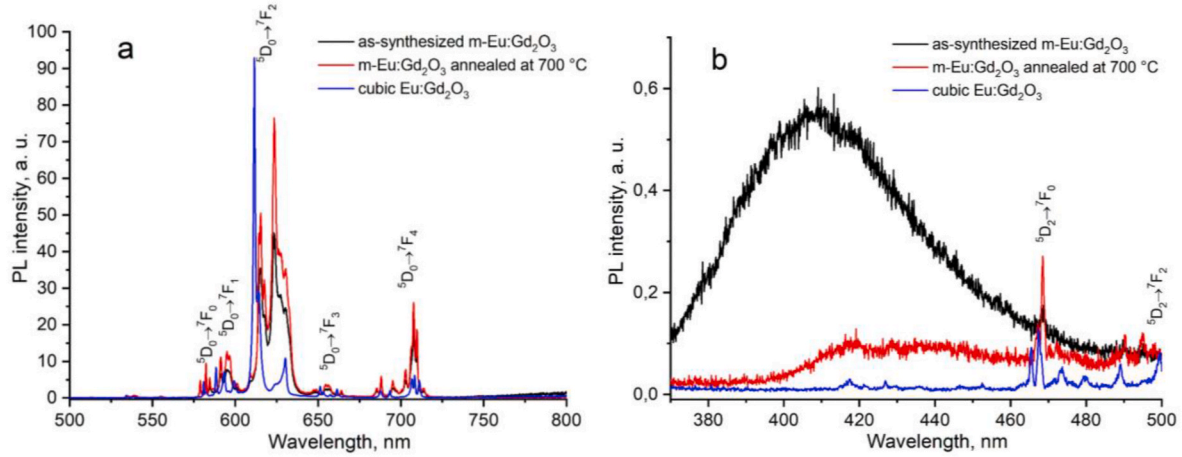

Fig. 6. The PL spectra of the as-synthesized m-Eu:Gd_2O_3 and m-Eu:Gd_2O_3 nanoparticles annealed at 700 °C and cubic Eu:Gd_2O_3 ($\lambda_{ex} = 270$ nm, T = 300 K). Luminescence bands originate from the $^5D_0$ starting level and terminate at ^7F_J levels, as indicated. PL spectra in the region of 370–500 nm are shown in more detail (b).

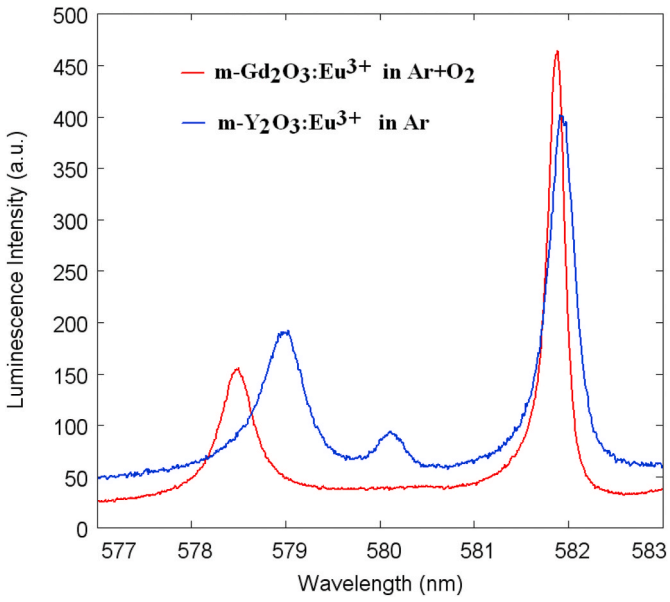

Fig. 7. The emission spectra of the m-Eu:Gd_2O_3 nanoparticles (red line, λ_{ex} = 408 nm, T = 300 K) in the spectral region of the ultra-narrow transition $^5D_0 \rightarrow {}^7F_0$. Blue line: luminescence of the monoclinic Eu:Y_2O_3 nanoparticles prepared in Ar [31].

mentioned above, all three inequivalent sites in Gd_2O_3 that can be occupied by Eu^{3+} ions are of C_s local symmetry. However, the degree of mirror symmetry violation at these sites can be different, and in case of nanoparticles obtained via vaporization, actual local symmetry can experience the influence of crystal structure defects. XRD from the nanoparticles evidently shows that their structure is monoclinic; however, it is not possible to determine in which positions Gd^{3+} ions are partially substituted by Eu^{3+} ions. This occurs because Gd^{3+} and Eu^{3+} ions differ only by one electron and are indistinguishable from each other in terms of XRD characteristics. Therefore, we examined the structure of the monoclinic Gd_2O_3 resolved in Ref. [39]. Really, among three different sites of Gd, the one specified as Gd3 in the paper cited above has a much smaller deviation from the geometrical center of GdO7 polyhedron. This center, when occupied by Eu^{3+}, must produce a reduced luminescence peak height and, moreover, in case of imperfect crystal structure within a nanoparticle, it is suspected to lose the mirror asymmetry. At the same time, two other Gd centers occupied by Eu show almost the same peak amplitudes of the luminescence, and both luminescence lines experience the same chemical shift to the blue, though the magnitude of this shift is different. From this observation, another explanation can be the suggested, namely, the prevalence of the Eu occupation of Gd sites with a stronger violation of the mirror symmetry. We believe that this is the case observed in our Eu:m-Gd_2O_3 nanoparticles, though, in fact, no decisive distinction between these two possible explanations can be done at present.

In the 588–605 nm spectral range the luminescence band is observed with three distinct components peaking at λ_{max} = 591.3, 595.0 and 601.0 nm. These lines are the components of magnetic dipole $^5D_0 \rightarrow {}^7F_1$ transition, the intensity of which is independent of the local symmetry of Eu ion. In the 605–644 nm range, the most intense luminescence band is positioned with the noticeable maximum at 623.5 nm (Fig. 6). Another intense line is positioned at λ_{max} = 615.0 nm, while less intense components are peaking at λ_{max} = 609.0 nm, λ_{max} = 618.0 nm, λ_{max} = 627.0 nm, and λ_{max} = 630.0 nm. These are the components of hypersensitive crystal-field-induced $^5D_0 \rightarrow {}^7F_2$ transition. The structure of $^5D_0 \rightarrow {}^7F_J$ luminescence band does not change after annealing of the Eu:m-Gd_2O_3 sample in accordance with XRD data. However, the improvement of the crystallinity, which can be suspected from the comparison of XRD patterns of as-synthesized and annealed nanophosphor, results in a two-fold growth in the intensity of the $^5D_0 \rightarrow {}^7F_2$ transition. In the cubic structure of lanthanide oxides, Eu^{3+} ions are located in two crystallographically nonequivalent sites with the six-fold coordination: one possessing C_2 point symmetry and another of S_6 site symmetry [4,5,7–16]. The most intense component of the $^5D_0 \rightarrow {}^7F_2$ transition of Eu^{3+} within the cubic structure of Gd_2O_3 is positioned at 611.0 nm [4,5,7–16]. In our starting target material Eu:c-Gd_2O_3, the $^5D_0 \rightarrow {}^7F_2$ transition maximizes at λ_{max} = 611 nm, Fig. 6. The chromaticity of phosphors based on Eu^{3+} is mainly determined by the $^5D_0 \rightarrow {}^7F_2$ transition. For as-synthesized m-Eu:Gd_2O_3 nanoparticles and for m-Eu:Gd_2O_3 nanoparticles annealed at 700 °C, the $^5D_0 \rightarrow {}^7F_2$ transition is maximized at 623.5 nm, with the red shift of about 12.5 nm as compared to cubic Eu:Gd_2O_3 samples. This indicates the possibility of applying the Eu:Gd_2O_3 nanoparticles obtained by laser vaporization as red nanophosphor with improved chromaticity. One may note from Fig. 6 that intensity of the electric dipole $^5D_0 \rightarrow {}^7F_2$ transition is noticeably higher than that of the magnetic dipole $^5D_0 \rightarrow {}^7F_2$ transition. This feature indicates a sufficient degree of inversion symmetry violation in the local environment of Eu^{3+} ions. The luminescence of m-Eu:Gd_2O_3 and m-Eu:Gd_2O_3 nanoparticles annealed at 700 °C in the 644–674 nm and 674–725 nm spectral ranges is due to $^5D_0 \rightarrow {}^7F_3$ and $^5D_0 \rightarrow {}^7F_4$ transitions of Eu^{3+} ions, respectively.

The weak PL band under excitation at 270 nm, which is detectable in the spectral region 370–500 nm with λ_{max} = 407 nm (Fig. 6b), can be attributed to the luminescence centers related to Eu^{2+} ions that possess the interconfigurational $4f^6 5\ d^1$ - $4f^7(^8S_{7/2})$ transition. The excitation channel of this transition looks like Eu^{2+} $(4f^7) + h\nu \rightarrow Eu^{2+*}$ $(4f^6 5d^1)$. Additionally, the 370–500 nm spectral range may also contain the luminescence of oxygen vacancies in different charge states. Anion vacancies in as-synthesized m-Gd_2O_3:Eu^{3+} may be associated with the charge compensation of Eu^{2+} ions within Gd_2O_3. We have established that Eu:Gd_2O_3 produced in the oxygen-containing environment exhibits a reduced luminescence from Eu^{2+} and an increased luminescence in the red region ($^5D_0 \rightarrow {}^7F_J$). Therefore, vaporization in the presence of oxygen reduces the content of oxygen vacancies, as one may expect. Similar effects can be observed after annealing of the sample in air, Fig. 6. In this case, the stoichiometry of m-Gd_2O_3 is also improved. Thus, if nanoparticles are intended for use as the red phosphor, the synthesis of nanoparticles should be carried out in the presence of oxygen for decreasing the contribution from the luminescence of Eu^{2+} ions. Similar results were obtained in our earlier study with Eu:Al_2O_3 nanoparticles [40]. This suggests that the PL properties of m-Gd_2O_3:Eu^{3+} and other oxide matrixes obtained by LAVA can be optimized through the careful control of the stoichiometry.

3.2.2. CIE coordinates

The CIE color chromaticity coordinates obtained from the PL spectra of m-Eu:Gd_2O_3 nanophosphor are marked on the CIE 1931 chromaticity diagram, Fig. 8.

The change in color of the emitted light from the samples was confirmed by the corresponding calculated color coordinates. The values of the color chromaticity coordinates (x, y) were found to be (x = 0.644; y = 0.325) for as-synthesized m-Eu:Gd_2O_3, (x = 0.659; y = 0.334) for m-Eu:Gd_2O_3 annealed at 700 °C, and (x = 0.649; y = 0.348) for cubic Eu:Gd_2O_3 (Fig. 8). The CIE values of the synthesized m-Gd_2O_3:Eu^{3+} samples fall in the red region. According to the National Television Standard Committee (NTSC), the ideal value of red color coordinates is (0.67, 0.33). This illustrates that m-Gd_2O_3:Eu^{3+} nanoparticles are suitable for the luminescent devices and applications.

3.2.3. Excitation study

Fig. 9 displays also the photoluminescence excitation (PLE) spectra recorded for the band with λ_{max} = 623.5 nm and for λ_{max} = 611 nm. The most intense band in the PLE spectrum ranges from 200 to 300 nm with the maximum at ca. 250 nm. This band originates from the charge transfer ($O^{2-} \rightarrow Eu^{3+}$) transition (LMCT). Previously [12], it was reported that LMCT lies in the indicated wavelength range both for cubic

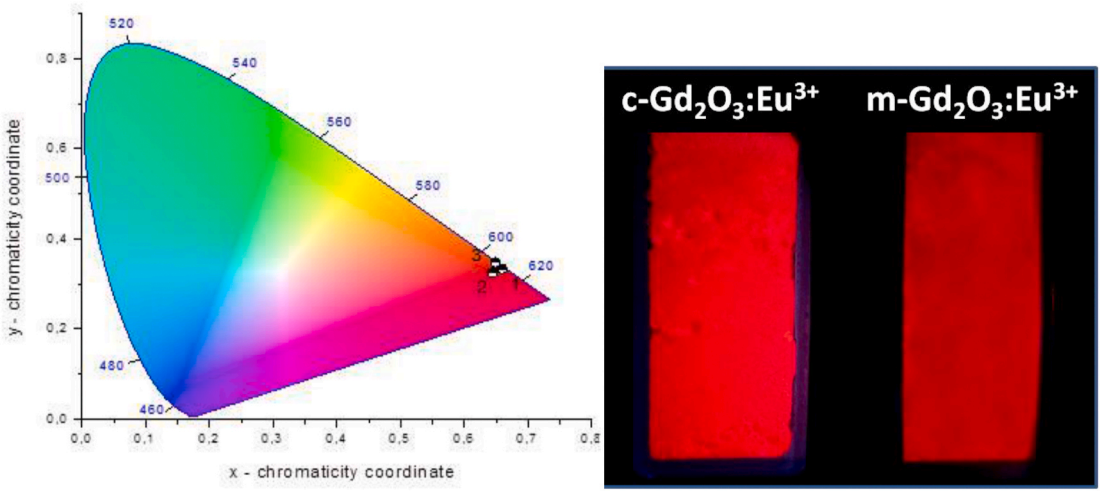

Fig. 8. The CIE 1931 coordinate for as-synthesized m-Gd_2O_3:Eu^{3+} (1), m-Gd_2O_3:Eu^{3+} annealed at 700 °C (2), and c-Gd_2O_3:Eu^{3+} (3) nanophosphors upon excitation at 270 nm (left) and a luminescence image of the as-synthesized Eu:Gd_2O_3 nanophosphor in a quartz cuvette under UV light excitation (Hg lamp irradiation at 365 nm) in contrast to the initial c-Gd_2O_3:Eu^{3+} phosphor.

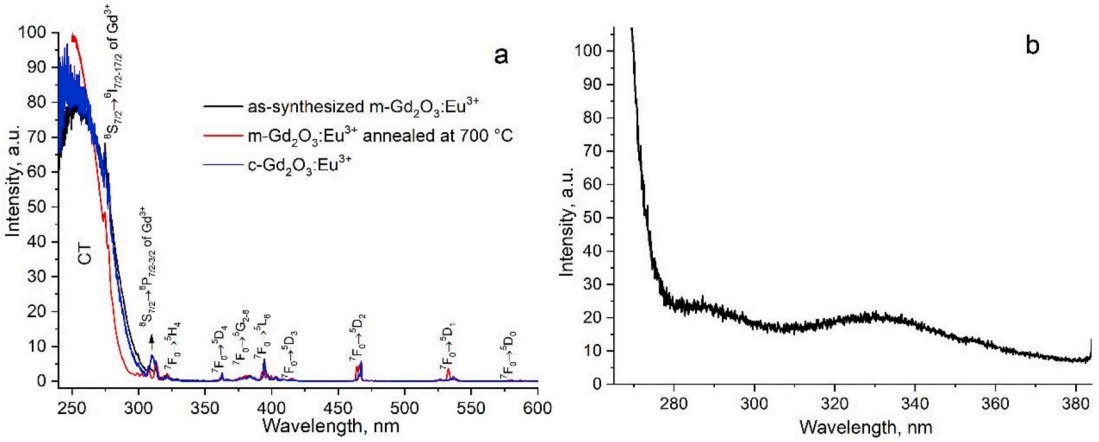

Fig. 9. a – PL excitation spectra of the as-synthesized m-Gd_2O_3:Eu^{3+}, m-Gd_2O_3:Eu^{3+} nanoparticles annealed at 700 °C, and c-Gd_2O_3:Eu^{3+} (λ_{em} = 623.5 and 611 nm, T = 300 K). b – The PL excitation spectrum of as-synthesized m-Gd_2O_3:Eu^{3+} nanoparticles (λ_{em} = 407 nm, T = 300 K).

and monoclinic Eu:Gd_2O_3. In the 320–600 nm range, the PLE spectrum contains narrow lines due to intraconfigurational *4f – 4f* transitions of Eu^{3+}. The 300–320 nm range reveals lines at λ_{max} = 307.2 nm and λ_{max} = 313.0 nm originating from intraconfigurational *4f – 4f* transitions of Gd^{3+}. The PLE spectrum of as-synthesized m-Gd_2O_3:Eu^{3+} nanoparticles, which was recorded for the band with λ_{em} = 407 nm, contains two broad bands with λ_{em} = 290 nm and λ_{em} = 330 nm that are assigned to Eu^{2+}. These bands are corresponding to the splitting of Eu^{2+} ion's 5d band in the m-Gd_2O_3 matrix.

3.2.4. PL quantum yield and decay study

The experimentally measured PLQY values at λ_{ex} = 395 nm for the as-synthesized m-Gd_2O_3:Eu^{3+} and m-Gd_2O_3:Eu^{3+} nanoparticles annealed at 700 °C were 1 and 4%, respectively. The acquired PLQY values are much lower than 26% and 21% obtained for the initial c-Gd_2O_3:Eu^{3+} phosphor and m-Y_2O_3:Eu^{3+} nanophosphor produced also by laser evaporation with similar particle sizes [31]. According to TG analysis, the samples contain a considerable amount of adsorbed OH, CO and CO_2 molecules, which are the main initiators of PL quenching. Obtained PLQY for laser-synthesized m-Gd_2O_3:Eu^{3+} is just the same as that earlier obtained for combustion-synthesized m-Gd_2O_3:Eu^{3+} with close values of europium concentration and nanoparticle sizes [17]. Therefore, employment of laser vaporization did not helped to overcome insufficient quantum efficiency of this system in comparison with combustion-synthesized m-Gd_2O_3:Eu^{3+}.

The PL kinetics for as-synthesized m-Gd_2O_3:Eu^{3+}, m-Gd_2O_3:Eu^{3+} nanoparticles annealed at 700 °C, and c-Gd_2O_3:Eu^{3+} samples was measured for the most intense band corresponding to the transition $^5D_0 \rightarrow {}^7F_2$ (λ_{em} = 623.5 and 611 nm) upon excitation at λ_{ex} = 270 nm, Fig. 10.

As seen in Fig. 10, the PL kinetics of the as-synthesized m-Gd_2O_3:Eu^{3+} (λ_{em} = 623.5) and m-Gd_2O_3:Eu^{3+} nanoparticles annealed at 700 °C is adequately described by the bi-exponential decay function:

$$I = A_1 e^{-t/\tau 1} + A_2 e^{-t/\tau 2},$$

where τ_1 and τ_2 are the lifetimes of the excited state $^5D_0$.

The corresponding lifetime values were $\tau_1 = 1.69*10^{-3}$ s and $\tau_2 = 0.24*10^{-3}$ s. Nanostructured oxide host matrices typically have two exponents in the PL kinetics of 4f activators [40–42]. The presence of several components is commonly attributed to the existence of several nonequivalent sites of impurity ions. The value for the "slow" component in PL kinetics is typical of the intrasite *f – f* transitions in Eu^{3+} ions. The presence of the "fast" component in PL kinetics testifies to the presence of an additional nonequivalent Eu^{3+} site in the structure of nanosized Gd_2O_3. In our case, these values strongly differ from each

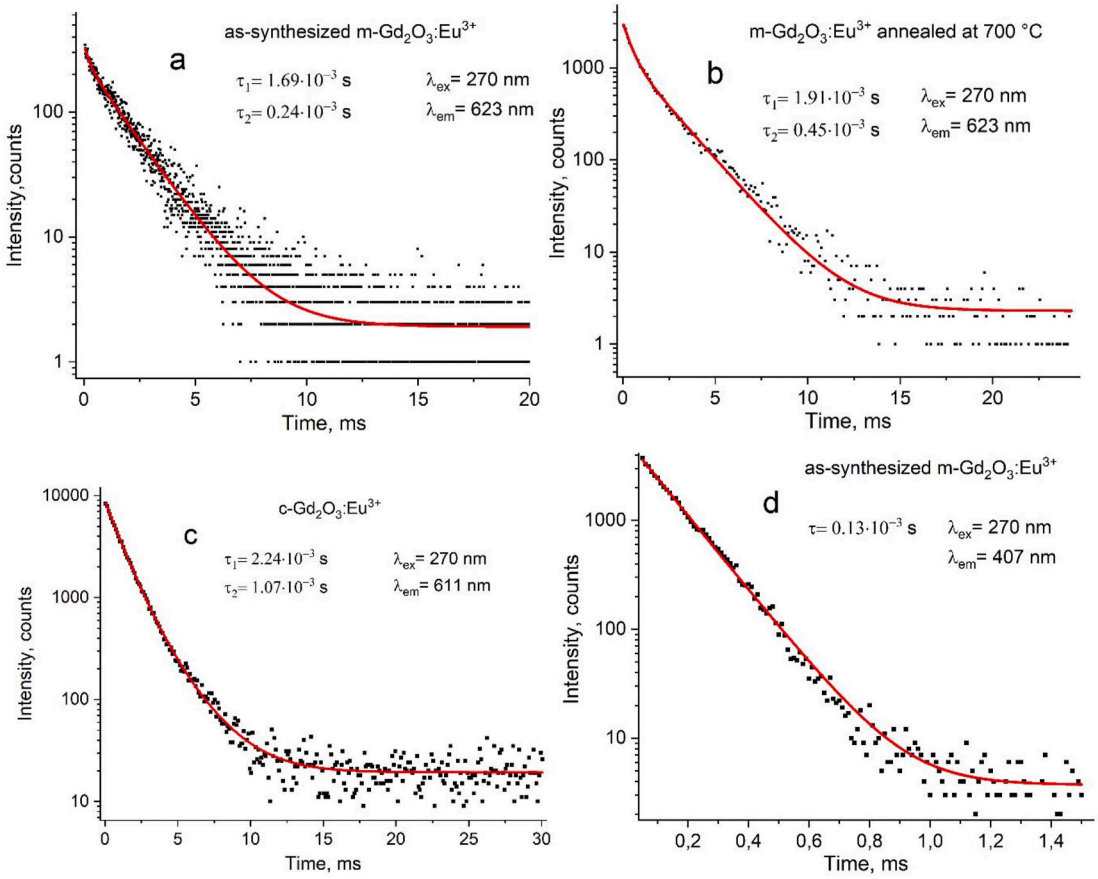

Fig. 10. Photoluminescence decay curves (log scale) of the as-synthesized m-Gd_2O_3:Eu^{3+} (λ_{em} = 623.5) (a), m-Gd_2O_3:Eu^{3+} nanoparticles annealed at 700 °C (λ_{em} = 623.5) (b), and c-Gd_2O_3:Eu^{3+} (λ_{em} = 611 nm) (c), λ_{ex} = 270 nm, T = 300 K. Photoluminescence decay curves (log scale) of the as-synthesized m-Gd_2O_3:Eu^{3+} (λ_{em} = 407 nm), λ_{ex} = 330 nm, T = 300 K (d).

other. So they can hardly be attributed to Eu^{3+} sites with the typical $^5D_0 \rightarrow {}^7F_0$ transitions that are displayed in Fig. 7. As shown in Ref. [41], Eu^{3+} ions in nanosized Y_2O_3 with the cubic crystal structure (the average particle size 40–50 nm) can reside in the normal (C_2 and C_{3i}) and defect sites, where they have strongly differing decay times. This suggests also that the "fast" component also corresponds to the defect sites. Most likely, in the case of Eu:Gd_2O_3 nanoparticles, defect sites of Eu^{3+} ions are located predominantly near the surface of nanoparticles, which has quite a high S_{sp} value of 60 m^2/g for the tested nanoparticles. After annealing, the decay time for both components increases to $\tau_1 = 1.91*10^{-3}$ s and $\tau_2 = 0.45*10^{-3}$ s due to the weakening of nonradiative processes. The results obtained are consistent with the data reported in Refs. [17,42]. The increase in the lifetime value after annealing of Gd_2O_3:Eu^{3+} samples was attributed to the particle size effect. For c-Gd_2O_3:Eu^{3+} phosphor, the kinetics is also described more adequately by the bi-exponential decay function with the typical lifetimes $\tau_1 = 2.24*10^{-3}$ s and $\tau_2 = 1.07*10^{-3}$ s. The PL kinetics of the as-synthesized m-Gd_2O_3:Eu^{3+} for the band with λ_{em} = 407 nm at λ_{ex} = 330 nm is described by exponential fitting with the lifetime $130*10^{-6}$ s. This value is typical of the interconfigurational $4f^7 \rightarrow 4f^6 5d^1$ transition to Eu^{2+}.

4. Conclusion

Europium doped Gd_2O_3 sphere-like nanoparticles with a specific surface area of 60 m^2/g were synthesized by cw CO_2 laser vaporization technique in a flowing mixture of argon and oxygen. According to HRTEM data, the Eu:Gd_2O_3 nanoparticles have a sphere-like shape and a high crystallinity. The size of Eu:Gd_2O_3 nanoparticles established by HRTEM is $d_m = 9.3 \pm 3.5$ nm, which is close to the coherent scattering region revealed by XRD. XRD analysis shows that laser vaporization enables crystallization of Eu:Gd_2O_3 nanoparticles in the crystal structure belonging to monoclinic symmetry class (*C2/m* space group). The most intense photoluminescence band in the red spectral region is attributed to the Eu^{3+} ions emission. Luminescence spectra of monoclinic Gd_2O_3:Eu^{3+} show a strong modification with respect to cubic Gd_2O_3:Eu^{3+}. The luminescence spectrum in the vicinity of the ultra-narrow $^5D_0 \rightarrow {}^7F_0$ transition of Eu^{3+} demonstrates only two peaks corresponding to two inequivalent positions of Eu^{3+} ion with C_s symmetry in the monoclinic Gd_2O_3 lattice that is explained by the peculiarities of local environment of Eu^{3+} ion at these sites. The hypersensitive transition $^5D_0 \rightarrow {}^7F_2$ with the maximum at 623.5 nm dominates in the spectrum and expands to the red part of the spectrum due to intense transitions terminating at higher-lying components of the crystal-field-split $^7F_2$ state. In the luminescence spectrum, an additional weak broad band with the maximum at 407 nm corresponding to electronic transitions $4f^6 5\,d^1(^7F_J) \rightarrow 4f^7(^8S_{7/2})$ of the Eu^{2+} was detected. The obtained luminescence excitation spectra and luminescence decay kinetics confirm this assignment. The obtained values of chromaticity coordinates and absolute quantum yield are (0.644; 0.325) and ca. 1%, respectively.

According to differential scanning calorimetry and thermogravimetry data, the single-phase monoclinic Eu:Gd_2O_3 is thermally stable up to a temperature of 900 °C. After annealing of Eu:Gd_2O_3 nanoparticles in air at 700 °C, the monoclinic symmetry class is preserved and the particle size increases to $d_m = 17.8 \pm 6.1$ nm. The chromaticity coordinates (0.659; 0.334) and absolute quantum yield (ca. 4%) obtained after annealing make it possible to use red phosphor based on monoclinic Gd_2O_3:Eu^{3+}. The CIE values of the synthesized m-Gd_2O_3:Eu^{3+} samples fall in the red region as compared with the initial Gd_2O_3:Eu^{3+} having the

cubic structure. Moreover, after annealing in air, the intensity of the Eu^{2+} luminescence band decreases.

Therefore, complete stabilization of the Eu^{3+} valence state in m-Gd_2O_3 is promising for creating a new source of red color for various applications, while optimization of the Eu^{3+}/Eu^{2+} content and excitation wavelength is the potential way for producing white phosphor. The lifetime of the excited $^5D_0$ state of Eu^{3+} in the as-synthesized nanoparticles is shorter than that in nanoparticles after annealing, due to the enhancement of nonradiative processes.

Author statement

A. I. Kostyukov: Conceptualization, Investigation, Writing - original draft, Project administration, V. N. Snytnikov: Investigation. Vl. N. Snytnikov: Investigation. M. I. Rakhmanova: Investigation. N. Y. Kostyukova: Investigation. A. V. Ishchenko: Investigation. S. V. Cherepanova: Investigation. A. S. Krylov: Investigation. A. S. Aleksandrovsky: Conceptualization, Formal analysis, Writing - original draft.

Declaration of competing interest

The authors declare that they have no known competing financial interests or personal relationships that could have appeared to influence the work reported in this paper.

Acknowledgment

The TEM studies are conducted using the equipment of the Center of Collective Use « National Center of Catalyst Research». This work is financially supported by the Russian Foundation for Basic Research (RFBR), Project no. 19-32-60027.

Appendix A. Supplementary data

Supplementary data to this article can be found online at https://doi.org/10.1016/j.jlumin.2021.118050.

References

[1] K. Binnemans, Interpretation of europium (III) spectra, Coord. Chem. Rev. 295 (2015) 1–45.
[2] P.A. Tanner, Some misconceptions concerning the electronic spectra of tripositive europium and cerium, Chem. Soc. Rev. 42 (2013) 5090–5101.
[3] N. Luo, C. Yang, X. Tian, J. Xiao, J. Liu, F. Chen, D. Zhang, D. Xu, Y. Zhang, G. Yang, D. Chen, L. Li, A general top-down approach to synthesize rare earth doped-Gd_2O_3 nanocrystals as dual-modal contrast agents, J. Mater. Chem. B 2 (2014) 5891–5897, 2.
[4] N.M. Maalej, A. Qurashi, A.A. Assadi, R. Maalej, M.N. Shaikh, M. Ilyas, M. A. Gondal, Synthesis of Gd_2O_3:Eu nanoplatelets for MRI and fluorescence imaging, Nanoscale Research Letters 10 (2015) 215 1–21510.
[5] D.K. Dosev, M.I. Nichkova, M. Liu, B. Guo, G. Liu, Y. Xia, B.D. Hammock, I. M. Kennedy, Application of luminescent Eu:Gd_2O_3 nanoparticles to the visualization of protein micropatterns, J. Biomed. Optic. 10 (6) (2005), 064006 1-7.
[6] F. Chen, Min Chen, Chuan Yang, J. Liu, N. Luo, G. Yang, D. Chen, Li Li, Terbium-doped gadolinium oxide nanoparticles prepared by laser ablation in liquid for use as a fluorescence and magnetic resonance imaging dual-modal contrast agent, Phys. Chem. Chem. Phys. 17 (2015) 1189.
[7] S.J. Park, J.Y. Park, H.K. Yang, Multi modality of hollow tube $Gd_2O_3:Eu^{3+}$ nanoparticles by using nonpolar solvent, J. Alloys Compd. 725 (2017) 807–817.
[8] Md W. Ahmad, W. Xu, S.J. Kim, J.S. Baeck, Y. Chang, J.E. Bae, K.S. Chae, J.A. Park, T.J. Kim, G.H. Lee, Potential dual imaging nanoparticle: Gd_2O_3 nanoparticle, Sci. Rep. 5 (2015) 1–11, 8549.
[9] E. Pavitra, J.S. Yu, A facile large-scale synthesis and luminescence properties of $Gd_2O_3:Eu^{3+}$ nanoflowers, Mater. Lett. 90 (2013) 134–137.
[10] R.G.A. Kumar, S. Hata, K.G. Gopchandran, Diethylene glycol mediated synthesis of $Gd_2O_3:Eu^{3+}$ nanophosphor and its Judd–Ofelt analysis, Ceram. Int. 39 (2013) 9125–9136.
[11] M. Buijs, A. Meyerink, G. Blasse, Energy transfer between Eu^{3+} ions in a lattice with two different crystallographic sites: $Y_2O_3:Eu^{3+}$, $Gd_2O_3:Eu^{3+}$ and Eu_2O_3, J. Lumin. 37 (1987) 9–20.
[12] Y.S. Vidya, K.S. Anantharaju, H. Nagabhushana, S.C. Sharma, Euphorbia tirucalli mediated green synthesis of rose like morphology of $Gd_2O_3:Eu^{3+}$ red phosphor: structural, photoluminescence and photocatalytic studies, J. Alloys Compd. 619 (2015) 760–770.
[13] J. Adam, W. Metzger, M. Koch, P. Rogin, T. Coenen, J.S. Atchison, P. König, Light emission intensities of luminescent Y_2O_3:Eu and Gd_2O_3:Eu particles of various sizes, Nanomaterials 7 (26) (2017) 1–17.
[14] O. Meza, E.G. Villabona-Leal, L.A. Diaz-Torres, H. Desirena, J.L. Rodríguez-Lopez, Elías Perez, Luminescence concentration quenching mechanism in $Gd_2O_3:Eu^{3+}$, J. Phys. Chem. 118 (2014) 1390–1396.
[15] C.-C. Lin, K.-M. Lin, Y.-Y. Li, Sol-gel synthesis and photoluminescent characteristics of Eu^{3+}-doped Gd_2O_3 nanophosphors, J. Lumin. 126 (2007) 795–799.
[16] Y.-J. Bae, K.-H. Lee, S.-H. Byeon, Synthesis and Eu^{3+} concentration-dependent photoluminescence of $Gd_{2-x}Eu_xO_3$ nanowires, J. Lumin. 129 (2009) 81–85.
[17] C. Liu, J. Liu, Judd-Ofelt intensity parameters and spectral properties of $Gd_2O_3:Eu^{3+}$ nanocrystals, J. Phys. Chem. B 110 (2006) 20277–20281.
[18] H.Y. Koo, S.H. Ju, D.S. Jung, S.K. Hong, D.Y. Kim, Y.C. Kang, Morphology control of Gd_2O_3:Eu phosphor particles with cubic and monoclinic phases prepared by high-temperature spray pyrolysis, Jpn. J. Appl. Phys. 45 (6A) (2006) 5018–5022.
[19] L.G. Jacobsohn, B.L. Bennett, R.E. Muenchausen, S.C. Tornga, J.D. Thompson, O. Ugurlu, D.W. Cooke, A.L. Lima Sharma, Multifunction nanocrystals produced by solution combustion synthesis: structural, luminescent, and magnetic characterization, J. Appl. Phys. 103 (2008), 104303 1-6.
[20] E.M. Goldys, K. Drozdowicz-Tomsia, S. Jinjun, D. Dosev, I.M. Kennedy, S. Yatsunenko, Marek Godlewski, Optical characterization of Eu-doped and undoped Gd_2O_3 nanoparticles synthesized by the hydrogen flame pyrolysis method, J. Am. Chem. Soc. 128 (2006) 14498–14505, 45.
[21] Y. Iwako, Y. Akimoto, M. Omiya, T. Ueda, T. Yokomori, Photoluminescence of cubic and monoclinic Gd_2O_3:Eu phosphors prepared by flame spray pyrolysis, J. Lumin. 130 (2010) 1470–1474.
[22] J. Dexpert-Ghys, M. Faucher, P. Caro, Site-selective excitation, crystal-field analysis, and energy transfer in europium-doped monoclinic gadolinium sesquioxide. A test of the electrostatic model, Phys. Rev. B 23 (1981) 607–617, 607.
[23] D.K. Rice, L.G. DeShazer, Spectra of europium in monoclinic gadolinium sesquioxide, J. Chem. Phys. 52 (1970) 172–178, 172.
[24] C. Liu, S. Lu, B. Chen, J. Zhang, J. Liu, The spectral properties of different structural centers in nanocrystalline $Gd_2O_3:Eu^{3+}$, J. Lumin. 122–123 (2007) 80–82.
[25] R. Kumar, M. Nyk, T.Y. Ohulchanskyy, C.A. Flask, P.N. Prasad, Combined optical and MR bioimaging using rare earth ion doped $NaYF_4$ nanocrystals, Adv. Funct. Mater. 19 (2009) 853–859.
[26] C.C. Huang, W. Huang, C.H. Su, C.N. Feng, W.S. Kuoa, C.S. Yeh, A general approach to silicate nanoshells: gadolinium silicate and gadolinium silicate: europium nanoshells for dual-modality optical and MR imaging, Chem. Commun. (2009) 3360–3362.
[27] C. Zollfrank, S. Gruber, M. Batentschuk, A. Osvet, F. Goetz-Neunhoeffer, S. Dittrich, J. Grabow, H.-D. Kurland, F.A. Müller, Synthesis of Eu-doped $SrAl_2O_4$ nanophosphors by CO_2 laser vaporization, Acta Mater. 61 (2013) 7133–7141.
[28] C. Wenisch, H.-D. Kurland, J. Grabow, F.A. Müller, Europium (III)-Doped $MgAl_2O_4$ spinel nanophosphor prepared by CO_2 laser co-vaporization, J. Am. Ceram. Soc. 99 (8) (2016) 2561–2564.
[29] A.I. Kostyukov, M.G. Baronskiy, T.V. Larina, V.N. Snytnikov, N.A. Zaitseva, A. A. Pochtar, A.V. Ishchenko, S.V. Cherepanova, V.N. Snytnikov, Laser vaporized CrO_x/Al_2O_3 nanopowders as a catalyst for isobutane dehydrogenation, Mater. Char. 169 (2020) 110664 1–11066414.
[30] A.I. Kostyukov, Vl N. Snytnikov, M.I. Rakhmanova, N.Y. Kostyukova, V. N. Snytnikov, Luminescent properties of $Al_2O_3:Tb^{3+}$ nanoparticles obtained by cw CO_2 laser vaporization, Opt. Mater. 110 (2020) 110508.
[31] A.I. Kostyukov, V.N. Snytnikov, Vl N. Snytnikov, A.V. Ishchenko, M. I. Rakhmanova, M.S. Molokeev, A.S. Krylov, A.S. Aleksandrovsky, Luminescence of monoclinic Y_2O_3:Eu nanophosphor produced via laser vaporization, Opt. Mater. 104 (2020) 109843.
[32] G. Skandan, C.M. Foster, H. Frase, M.N. Ali, J.C. Parker, H. Hahn, Phase characterization and stabilization due to grain size effects of nanostructured Y_2O_3, Nanostruct. Mater. 1 (1992) 313–322.
[33] B. Bihari, H. Eilers, B.M. Tissue, Spectra and dynamics of monoclinic Eu_2O_3 and $Eu^{3+}:Y_2O_3$ nanocrystals, J. Lumin. 75 (1997) l–10.
[34] M. Mishra, P. Kuppusami, S. Ramya, V. Ganesan, A. Singh, R. Thirumurugesan, E. Mohandas, Microstructure and optical properties of Gd_2O_3 thin films prepared by pulsed laser deposition, Surf. Coating. Technol. 262 (2015) 56–63.
[35] T. Thongtem, A. Phuruangrat, D.J. Ham, J.S. Lee, S. Thongtem, Controlled Gd_2O_3 nanorods and nanotubes by the annealing of $Gd(OH)_3$ nanorod and nanotube precursors and self-templates produced by a microwave-assisted hydrothermal process, CrystEngComm 12 (2010) 2962–2966.
[36] H. Guoa, X. Yang, T. Xiao, W. Zhang, L. Lou, Jacques Mugnier, Structure and optical properties of sol–gel derived Gd_2O_3 waveguide films, Appl. Surf. Sci. 230 (2004) 215–221.
[37] J.-G. Kang, B.-K. Min, Y. Sohn, Synthesis and characterization of $Gd(OH)_3$ and Gd_2O_3 nanorods, Ceram. Int. 41 (2015) 1243–1248.
[38] M.G. Ivanov, I.V. Krutikova, U. Kynast, M. Lezhnina, I.S. Puzyrev, Laser-synthesized $Y_2O_3:Eu^{3+}$ nanophosphors and their stabilization in water suspensions, Opt. Mater. 74 (2017) 67–75.
[39] F.X. Zhang, M. Lang, J.W. Wang, U. Becker, R.C. Ewing, Structural phase transition of cubic Gd_2O_3 at high pressures, Phys. Rev. B 78 (2008), 064114.
[40] A.I. Kostyukov, Vl N. Snytnikov, A.V. Zhuzhgov, S.V. Cherepanova, A. V. Ishchenko, M.G. Baronskiy, V.N. Snytnikov, Size-dependent photoluminescence

of europium in alumina nanoparticles synthesized by cw CO_2 laser vaporization, J. Alloys Compd. 815 (2020) 152476.

[41] I.E. Kolesnikov, A.V. Povolotskiy, D.V. Mamonova, E. Lahderanta, A.A. Manshina, M.D. Mikhailov, Photoluminescence properties of Eu^{3+} ions in yttrium oxide nanoparticles: defect vs. normal sites, RSC Adv. 6 (2016) 76533.

[42] R.S. Ningthoujam, R. Shukla, R.K. Vatsa, V. Duppel, L. Kienle, A.K. Tyagi, Gd_2O_3: Eu^{3+} particles prepared by glycine-nitrate combustion: phase, concentration, annealing, and luminescence studies, J. Appl. Phys. 105 (2009), 084304.